Low-order mode correction anisoplanatism limitations for adaptive optics system

Hongtao Zhang
Fuchang Yin
Changchun Institute of Optics and Fine Mechanics
Changchun, China

Bing Xu, MEMBER SPIE
Wenhan Jiang, MEMBER SPIE
The Chinese Academy of Sciences
Institute of Optics and Electronics
Chengdu, China

Abstract. Anisoplanatism error for the low-order mode and its influence on compensation effects are analyzed both theoretically and experimentally. For non-Kolmogorov turbulence, the anisoplanatism error, the angular correlation function of Zernike polynomials, the long-exposure optical transfer function (OTF), and the residual phase structure function are all discussed. The modal correction coefficient is used to evaluate the influence of anisoplanatism error on the compensation effectiveness of an adaptive optics system used as the low-order mode correction. The numerical calculation results of the modal correction coefficient and long-exposure OTF for light beam horizontal atmospheric propagation are also presented. © *2003 Society of Photo-Optical Instrumentation Engineers.*
[DOI: 10.1117/1.1588295]

Subject terms: non-Kolmogorov turbulence; long-exposure optical transfer function; anisoplanatism error; modal correction coefficient.

Paper 020446 received Oct. 11, 2002; revised manuscript received Dec. 26, 2002; accepted for publication Jan. 16, 2003.

1 Introduction

Adaptive optics is a technique used to measure and correct the optical wavefront distortions induced by atmospheric turbulence in real time.[1–3] The principle of adaptive optics is to improve the image quality of optical and IR astronomical telescopes, to image and track moving space objects rapidly, and to compensate for laser beam distortion through the turbulent atmosphere. Although the Kolmogorov formulation has been widely used to describe atmospheric turbulence, there are some turbulence conditions that experimental data do not support. If the turbulence is modeled as Kolmogorov and is actually non-Kolmogorov through a portion of the atmosphere, the performance of these adaptive optics systems will be degraded. The Kolmogorov model defined by 3-D power spectral density is a statistical model for the variations of the index of refraction

been established at the Yunnan Observatory (see Fig. 1). The atmospheric turbulent disturbance data were measured by a Shack-Hartmann wavefront sensor, according to the experimental data processing; this proved that the atmospheric turbulence did not obey the Kolmogorov law during most of the observation time. The temporal power spectrum of the wavefront disturbance in the high-frequency domain is proportional to −1.6 to 2 squared which greatly deviates from the Kolmogorov law of −8/3 squared. Some experimental data collected on March 23, 2000, are given in Fig. 2.

Buser made measurements of the turbulence power spectra in the Earth's boundary layer using a three-beam Mach-Zender optical interferometer.[5] By having several laser beams propagating at different paths through the turbulence interfere and analyzing the interferograms, Buser found that the Kolmogorov theory did not support his mea-

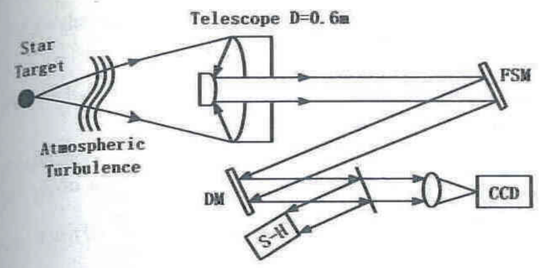

Fig. 1 Star observation with adaptive optics system. The deformable mirror actuator unit is 61, the effective subaperture number is 48, the sampling frequency is 838 Hz, and time delay is 2.8 s. FSM, fast steering mirror; DM, deformable mirror; and S-H, Shack-Hartmann sensor.

can be applied without significant error anywhere else inside the region. Whereas a size that is determined in this way is almost certain to be small enough, the problem is that it is an unnecessarily stringent requirement that does not account for the actual properties of optical systems. An important practical consideration in the use of adaptive optics is that the real atmospheric compensation system can detect and respond to changing conditions only at a finite rate. A common assumption is that, for atmospheric conditions that are characterized by a temporal spectrum $\Phi(f)$, the residual error is given by

$$\sigma_r^2=\int_0^\infty df\Phi(f)\frac{(f/f_{3dB})^2}{1+(f/f_{3dB})^2}, \tag{2}$$

where f_{3dB} is the characteristic frequency of a first-order correction system.

Greenwood and Fried analyzed bandwidth considerations for atmospheric turbulence. Greenwood's[7] commonly used expression for the characteristic frequency that is required to achieve a given residual error can be shown to be equivalent to including the atmospheric piston within the aperture as part of the residual error, and its use therefore tacitly assumes that the piston error has a degrading effect on the optical system. Tilt is also included, and if it is corrected by a separate tracking system, its inclusion may also be undesirable. In the following, we define a model correction factor for the residual error that correctly accounts for these effects and that one can therefore use to obtain a better estimate for the compensation effect in correcting an adaptive optics system.

If the incoming wavefront of the beacon and the observing telescope of an adaptive optics system are not in the same direction, a bright star or laser guide star is usually used to provide a reference, and then the positive residual errors in the system will include anisoplanatism error besides the errors induced by limiting bandwidth and detecting noise. Among the preceding wavefront errors, the low-order Zernike modes account for the major parts. For the Kolmogorov law, the percentage of the Zernike-coefficient variances of the first-order (tip-tilt) modes and the second-order (defocus and astigmatism) modes are 86.9 and 6.7%, respectively. Therefore the compensation of an adaptive optics system is effective even if only the low-order modes of wavefront disturbance are corrected. For the limitations of compensation, the effects caused by limiting bandwidth and detecting noise are detailed (see Ref. 8), and anisoplanatism-based errors are carefully considered as discussed here.

Assume an angular interval between an incoming wavefront of a beacon and the telescope observation target direction is a, and an incoming wavefront $\phi(R\mathbf{x},a)$ can be expressed as

$$\begin{aligned}\phi(R\mathbf{x},a)&=\sum_{j=2}^{\infty}a_j(a)Z_j(\mathbf{x})\\&=\sum_{j=2}^{N}a_j(a)Z_j(\mathbf{x})+\sum_{j=N+1}^{\infty}a_j(a)Z_j(\mathbf{x})\\&=\phi_L(R\mathbf{x},a)+\phi_H(R\mathbf{x},a),\end{aligned} \tag{3}$$

where R is the observing system radius (D is its diameter), $\mathbf{x}$ is a 2-D coordinate, $Z_j(\mathbf{x})$ are Zernike polynomials, j is the modal ordinal number, and $a_j(a)$ is modal coefficient of atmospheric turbulence, and

$$\varphi_\varepsilon(R\mathbf{x},a)=\phi_{\varepsilon_L}(R\mathbf{x},a)+\phi_{\varepsilon_H}(R\mathbf{x},a)$$
$$=\sum_{j=2}^{N}[a_j(a)-a_j(0)]Z_j(\mathbf{x})$$
$$+\sum_{j=N+1}^{\infty}a_j(a)Z_j(\mathbf{x}), \tag{7}$$

and

$$\phi_{\varepsilon_L}(R\mathbf{x},a)=\sum_{j=2}^{N}[a_j(a)-a_j(0)]Z_j(\mathbf{x})=\sum_{j=2}^{N}\varepsilon_j(a)Z_j(\mathbf{x}), \tag{8}$$

where $\phi_{\varepsilon_L}(R\mathbf{x},a)$ is the residual phase of low-order mode, and $\varepsilon_j(a)=a_j(a)-a_j(0)$ is the low-order modal coefficient caused by anisoplanatism. Under the condition of generalized smoothness, the wavefront residual error anisoplanatism induced after low-order-mode compensation can be expressed as

$$\sigma_\phi^2(a)=\sum_{j=2}^{N}\varepsilon_j^2(a)+\sum_{j=N+1}^{\infty}\langle a_j^2(0)\rangle$$
$$=2\sum_{j=2}^{N}[a_j^2(0)-\langle a_j(a)a_j(0)\rangle]$$

and

$$W(\mathbf{x})Z_j(\mathbf{x})=\int\int \mathrm{d}^2\mathbf{K}Q_j(K,\varphi)\exp(-2i\pi\mathbf{K}\cdot\mathbf{x}), \tag{13}$$

where $K=|\mathbf{K}|$, $\mathbf{K}$ is the 2-D spatial frequency domain coordinate, and $Q_j(K,\varphi)$ is the Fourier transform of $Z_j(x)$, which can be expressed as

$$Q_j(K,\varphi)=(n+1)^{1/2}\frac{J_{n+1}(2\pi K)}{\pi K}$$
$$\times\begin{cases}(-1)^{(n-m)/2}i^m\sqrt{2}\cos(m\varphi) & j=\text{even},m\neq 0\\ (-1)^{(n-m)/2}i^m\sqrt{2}\sin(m\varphi) & j=\text{odd},m\neq 0\\ (-1)^{n/2} & m=0,\end{cases} \tag{14}$$

where J_n is the Bessel function of the n'th order. Substituting Eq. (13) for Eq. (12), we can obtain

$$\langle a_j(a)a_j(0)\rangle=\int\int \mathrm{d}^2\mathbf{K}_1\int\int \mathrm{d}^2\mathbf{K}_2Q_j(K_1,\varphi_1)$$
$$\times Q_j^*(K_2,\varphi_2)\int\int \mathrm{d}^2\mathbf{x}_1\int\int \mathrm{d}^2\mathbf{x}_2$$
$$\times\exp(-2i\pi\mathbf{K}_1\cdot\mathbf{x}_1)\exp(2i\pi\mathbf{K}_2\cdot$$

Notice that if

$$\delta(\mathbf{K}_2-\mathbf{K}_1)=\int\int \mathrm{d}^2\mathbf{x}_2\exp[2i\pi(\mathbf{K}_2-\mathbf{K}_1)\cdot\mathbf{x}_2], \tag{19}$$

then $\langle a_j(a)a_j(0)\rangle$ can be expressed as

$$\langle a_j(a)a_j(0)\rangle=\sum_l\int\int \mathrm{d}^2\mathbf{K}Q_j(K;\varphi)Q_j^*(K,\varphi)$$
$$\times\int\int \mathrm{d}^2\mathbf{x}\exp(2i\pi\mathbf{K}\cdot\mathbf{x})$$
$$\times B_{\phi l}[R\chi(z)\mathbf{x}-azi]. \tag{20}$$

Since the autocorrelation function and power spectrum take the form of a Fourier transform,

$$\langle a_j(a)a_j(0)\rangle=\sum_l\frac{1}{R^2}\int\int \mathrm{d}^2\mathbf{K}Q_j(K,\varphi)Q_j^*(K,\varphi)$$
$$\times\exp\left[2i\pi\frac{az}{R\chi(z)}\mathbf{K}\cdot\mathbf{i}\right]W_{\phi l}\left[\frac{K}{R\chi(z)}\right], \tag{21}$$

where $W_{\phi l}[K/R\chi(z)]$ is the phase power spectrum located in the l'th turbulent layer. The normalized phase power

$$b_{n,m}\left(\frac{az}{R}\mathbf{K}\cdot\mathbf{i}\right)=\int_0^{2\pi}\mathrm{d}\varphi\exp\left(i2\pi\frac{az}{R}K\cos\varphi\right)q_j, \tag{26}$$

$$q_j=\begin{cases}(-1)^{n-m}2\cos^2(m\varphi) & j=\text{even},\ m\neq 0\\ (-1)^{n-m}2\sin^2(m\varphi) & j=\text{odd},\ m\neq 0\\ (-1)^n & m=0\end{cases}. \tag{27}$$

Notice that

$$\int_0^{2\pi}\mathrm{d}\theta\exp(jz\cos\theta)\cos(n\theta)=2\pi(-1)^{(3/2)n}J_n(z). \tag{28}$$

From the preceding, the angular correlation coefficient for a Zernike polynomial can finally be expressed as

$$\langle a_j(a)a_j(0)\rangle$$
$$=8(n+1)\pi^{\beta-1}A_\beta\left(\frac{D}{\rho_0}\right)^{\beta-2}$$
$$\times\frac{\int_0^L\mathrm{d}zC_n^2(z)[\chi(z)]^{\beta-2}I_{n,m}\{[az/R\chi(z)],\beta\}}{\int_0^L\mathrm{d}zC_n^2(z)[\chi(z)]^{\beta-2}}, \tag{29}$$

where ρ_0 is a parameter indicating atmospheric turbulence

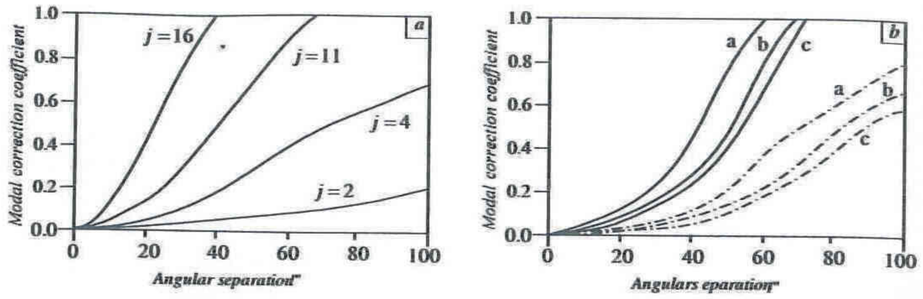

Fig. 3 Modal correction coefficient as function of the angular separation for 1000-m horizontal atmospheric propagation: (a) $\beta=44/12$; (b) solid line: $j=11$, dash-dotted line: $j=4$, the curves in the figure denote a, $\beta=40/12$; b, $\beta=44/12$; and c, $\beta=46/12$, respectively.

phase structure functions, respectively. The high-order modal residual phase structure function is analyzed in Ref. 11, and is not illustrated here. According to Eq. (8), the low-order modal residual phase structure function can be derived easily as

$$D_{\phi_{\varepsilon_L}}(\mathbf{u},a)=\frac{\iint W(\mathbf{x})W(\mathbf{x}+\mathbf{u})\langle\{\phi_{\varepsilon_L}(R\mathbf{x},a)-\phi_{\varepsilon_L}[R(\mathbf{x}+\mathbf{u}),a]\}^2\rangle\,\mathrm{d}^2\mathbf{x}}{\iint W(\mathbf{x})W(\mathbf{x}+\mathbf{u})\mathrm{d}^2\mathbf{x}}=\sum_{j=2}^{N}\varepsilon_j^2(a)d_j(\mathbf{u}), \tag{34}$$

where $d_j(\mathbf{u})$ is a shape function

$$d_j(\mathbf{u})=\frac{\iint W(\mathbf{x})W(\mathbf{x}+\mathbf{u})[Z_j(\mathbf{x})-Z_j(\mathbf{x}+\mathbf{u})]^2\,\mathrm{d}^2\mathbf{x}}{\iint W(\mathbf{x})W(\mathbf{x}+\mathbf{u})\,\mathrm{d}^2\mathbf{x}}. \tag{35}$$

For low-order modes, the shape function has simple analytical expressions

$$d_2(\mathbf{u})=d_3(\mathbf{u})=8u^2,$$
$$d_4(\mathbf{u})=2d_5(\mathbf{u})=2d_6(\mathbf{u})=48u^2(1-u)^2. \tag{36}$$

According to the preceding derivations and Ref. 12, the residual phase structure function and long-exposure OTFafter low-order-mode correction can be expressed, respectively, as

$$D_{\phi_\varepsilon}(\mathbf{u},a)=D_\phi(\mathbf{u})-\sum_{j=2}^{N}\langle a_j^2(0)\rangle d_j(\mathbf{u})+\sum_{j=2}^{N}\langle\varepsilon_j^2(a)\rangle d_j(\mathbf{u}), \tag{37}$$

$$\tau(\mathbf{u},a)=\tau_0(\mathbf{u})\exp[-\tfrac{1}{2}D_{\phi_\varepsilon}(\mathbf{u},a)], \tag{38}$$

and

$$\langle a_j^2(0)\rangle=\frac{(n+1)\Gamma(2n+2-\beta/2)\Gamma(\beta+4/2)\Gamma(\beta/2)\sin\{[\pi(\beta-2)/2]\}}{\pi\Gamma(2n+4+\beta/2)}\times\left(\frac{D}{\rho_0}\right)^{\beta-2}, \tag{39}$$

$$D_\phi(\mathbf{u})=\overline{|\phi(\mathbf{x},t)-\phi(\mathbf{x}+\mathbf{u},t)|^2}=\gamma_\beta(D/\rho_0)^{\beta-2}u^{\beta-2}, \tag{40}$$

where γ_β is a structure constant, and can be expressed as

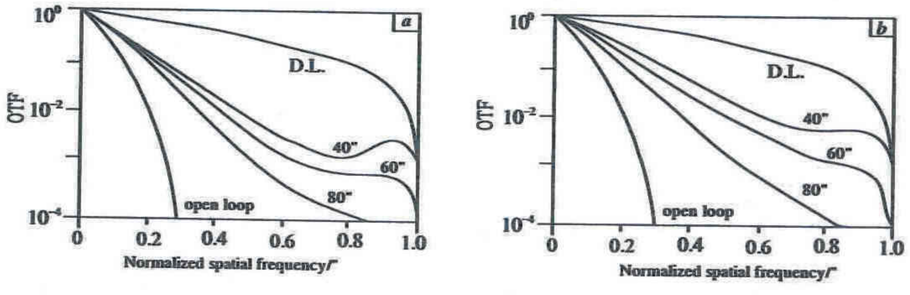

Fig. 4 Long-exposure OTF after the low-order-mode correction for the different angular separations; $D=0.6$ m, $\rho_0=10$ cm, $\beta=44/12$, and $L=1000$ m: (a) tip-tilt correction; and (b) tip-tilt, defocus, and astigmatism correction. Here D.L. is diffraction limit.

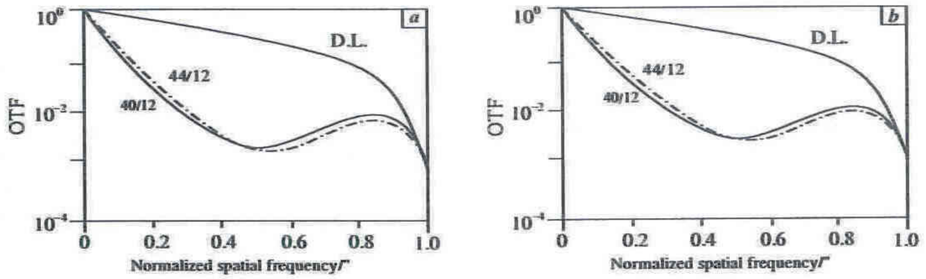

Fig. 5 Long-exposure OTF after low-order-mode correction for different values of β; $D=0.6$ m, $\rho_0=10$ cm, $a=10"$, and $L=1000$ m: (a) tip-tilt correction and (b) tip-tilt, defocus, and astigmatism correction. Here D.L. is diffraction limit.

$$\gamma_\beta=\frac{2^{\beta-1}[\Gamma(\beta+2/2)]^2\Gamma(\beta+4/2)}{\Gamma(\beta/2)\Gamma(\beta+1)}. \tag{41}$$

For the Kolmogorov spectrum, $\gamma_{11/3}=6.88$.

5 Numerical Calculation Results for Horizontal Transmission of Light Waves

When light waves propagate along the horizontal atmosphere, $C_n^2(z)=C_n^2$ is a constant, and then the Zernike angular correlation function can be expressed as

$$\langle a_j(a)a_j(0)\rangle=8(n+1)\pi^{\beta-1}A_\beta(\beta-1)^{-1}\left(\frac{D}{\rho_0}\right)^{\beta-2}\times\int_0^1\mathrm{d}z(1-z)^{\beta-2}I_{n,m}\left[\frac{azL}{R(1-z)},\beta\right]. \tag{42}$$

Figure 3 shows functional relation curves calculated from different propagating modes and modal correction factor β and angular spacing a according to Eqs. (11) and (42) for horizontal atmospheric transmission of light waves. Figure 3(a) shows the curves of the functional relationship between β and a when j is 2, 4, 11, and 16 for Kolmogorov turbulence at $\beta=44/12$, and Fig. 3(b) shows the curves of β and a for j equals to 4 (dash-dotted line) and 11 (solid line) with different values of β (40/12, 44/12, and 46/12).

Figures 4, 5, and 6 are long-exposure OTF curves of different a, β, and ρ_0 values obtained after the low-order modes were corrected for the horizontal atmospheric transmission system. Note that the overcorrection phenomenon will occur at the high-frequency band of the long-exposure OTF curve after low-order-mode correction because we did not consider modal coupling. Reference 13 once posed this phenomenon. Modal coupling has little influence on the long-exposure OTF curve at a lower frequency band. It influences only the high-frequency band of the long-exposure OTF curve and has little influence for calculation of a long-exposure image Strehl ratio (SR) and full width at half maximum (FWHM). To eliminate the overcorrection phenomenon, we used a method in this paper is similar to that used in Ref. 14. According to Eqs. (36), (37), and (40), the residual phase structure function after correction for tip-tilt, defocus, and astigmatism can be obtained as

$$D_{\phi_\varepsilon}(\mathbf{u},a)=\gamma_\beta(D/\rho_0)^{\beta-2}u^{\beta-2}(1-Au^{4-\beta}), \tag{43}$$

$$D_{\phi_\varepsilon}(\mathbf{u},a)=\gamma_\beta(D/\rho_0)^{\beta-2}u^{\beta-2}\times[1-Au^{4-\beta}-Bu^{4-\beta}(1-u)^2], \tag{44}$$

and

$$A=16[\langle a_2^2(0)\rangle-\langle\varepsilon_2^2(a)\rangle]/\gamma_\beta,$$
$$B=96[\langle a_4^2(0)\rangle-\langle\varepsilon_4^2(a)\rangle]/\gamma_\beta. \tag{45}$$

When $A>1$, we select $A=1$, and when $B>1$, we selection $B=1$. Then the overcorrection phenomenon can be eliminated.

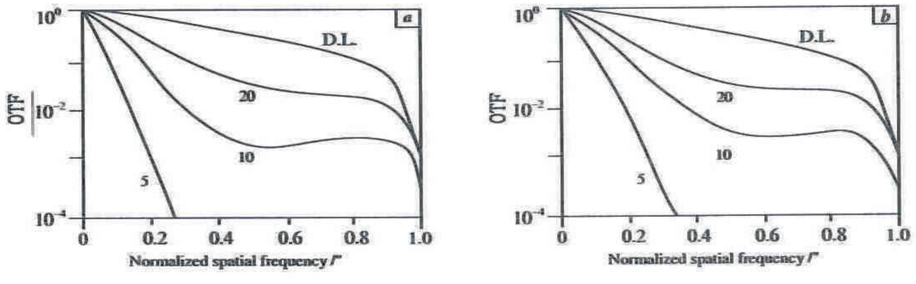

Fig. 6 Long-exposure OTF after low-order-mode correction for different values of ρ_0; $D=0.6$ m, $\beta=44/12$, $a=50"$, and $L=1000$ m: (a) tip-tilt correction and (b) Tip-tilt, defocus, and astigmatism correction.

6 Conclusions

The theoretical laws of anisoplanatism errors, the modal correction factor, the angular correlation function of the Zernike coefficient, the residual phase structure function, and the long-exposure OTF after low-order-mode correction were all analyzed under non-Kolmogorov turbulence. It was shown that the modal correction factor will increase with higher modal orders at the same angular intervals a and normalized exponent decreases of the phase spectrum spatial frequency β. At the same time that the correction effect is worsens, the modal correction factor will increase with the larger a at the same mode and β, and the system also has a worse correction effect. The modal correction factor will decrease with the higher β at the same mode and a, and system has a better correction effect. Finally, a better correction effect can be obtained with the increased ρ_0 (which familiar to atmospheric coherent constant r_0) at the same a, β, and correction modes.

References

1. W. H. Jiang, M. Q. Li, and G. M. Tang, "Adaptive optics image compensation experiments for star objects," *Opt. Eng.* 34(1), 15–20

use of Zernike polynomials and Karhumen-Loeve functions," *J. Opt. Soc. Am.* 12(10), 2182–2193 (1995).

14. J. Y. Wang, "Optical resolution through a turbulent medium with adaptive phase compensation," *J. Opt. Soc. Am.* 63(3), 383–390 (1977).

Hongtao Zhang received his BA and MA degrees in optical measuring technology from Changchun Institute of Optics and Fine Mechanics and Jilin University in 1992 and 2000, respectively. In 1992 he joined the Army in the Armor Technology Institute of PLA, working on research and development tools for optically based weapon equipment. He is currently a doctoral student in optical engineering at Changchun Institute of Optics and Fine Mechanics, and will graduate on June 2003. He specializes in the field of space laser communication systems with adaptive optics.

Fuchang Yin directs the Optics Academy in Jilin Province. He is an expert in the field of space laser communication systems and target identification. He successfully developed several momentous projects, such as the laser target identification

Axicon as a retroreflector in open-path Fourier transform infrared spectrometry

Robert L. Richardson
Peter R. Griffiths*
University of Idaho
Department of Chemistry
Moscow, Idaho 83844-2343

Abstract. Ray-tracing analysis of a particular reflecting axicon, a right circular cone, for use as a retroreflector in active open-path Fourier-transform IR (OP/FT-IR) spectrometry, and the results of testing a 0.305-m aperture right circular cone using a commercial active OP/FT-IR spectrometer are presented. The ray-tracing model is based on the optical characteristics of a commercial single-telescope monostatic OP/FT-IR spectrometer and models the off-axis behavior normally encountered under practical field conditions during field use. Of practical concern are the trends for the diameter of the beam reflected from the retroreflector as a function of the path length between spectrometer and retroreflector and misalignment of the retroreflector with respect to the transmitted beam. Construction and the results of field-testing two smaller epoxy-composite axicons replicated from the 0.305-m master are presented.

[DOI: 10.1117/1.1597566]